PAPER

A novel pendulum test for measuring roller chain efficiency

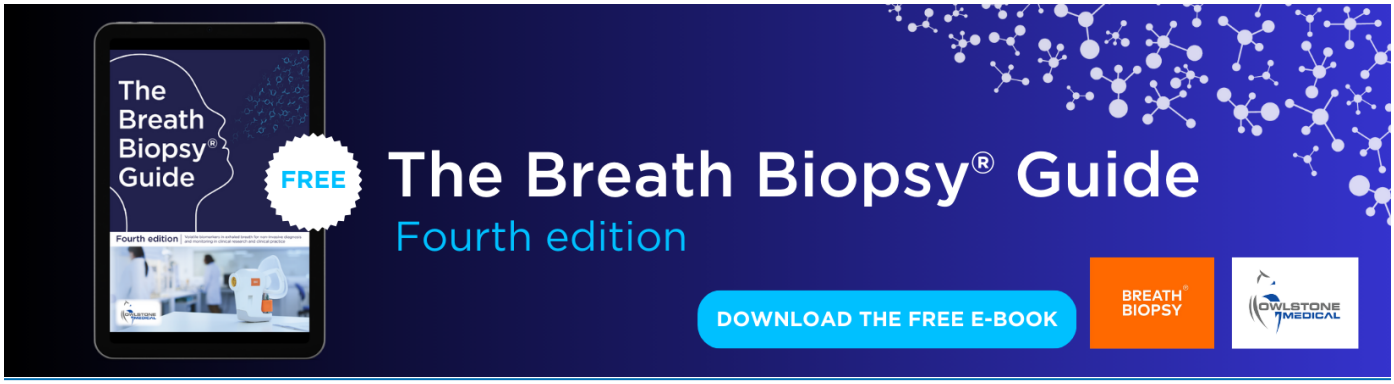

IOP Publishing Measurement Science and Technology
Meas. Sci. Technol. **29** (2018) 075008 (12pp) https://doi.org/10.1088/1361-6501/aaa239

A novel pendulum test for measuring roller chain efficiency

R Wragge-Morley, J Yon, R Lock, B Alexander and S Burgess

Department of Mechanical Engineering, University of Bristol, Queens Building, University Walk, Bristol BS8 1TR, United Kingdom

E-mail: rw8529@bristol.ac.uk

Received 9 August 2017, revised 5 December 2017
Accepted for publication 15 December 2017
Published 29 May 2018

Abstract

This paper describes a novel pendulum decay test for determining the transmission efficiency of chain drives. The test involves releasing a pendulum with an initial potential energy and measuring its decaying oscillations: under controlled conditions the decay reveals the losses in the transmission to a high degree of accuracy. The main advantage over motorised rigs is that there are significantly fewer sources of friction and inertia and hence measurement error. The pendulum rigs have an accuracy around 0.6% for the measurement of the coefficient of friction, giving an accuracy of transmission efficiency measurement around 0.012%. A theoretical model of chain friction combined with the equations of motion enables the coefficient of friction to be determined from the decay rate of pendulum velocity. The pendulum rigs operate at relatively low speeds. However, they allow an accurate determination of the coefficient of friction to estimate transmission efficiency at higher speeds. The pendulum rig revealed a previously undetected rocking behaviour in the chain links at very small articulation angles. In this regime, the link interfaces were observed to roll against one another rather than slide. This observation indicates that a very high-efficiency transmission can be achieved if the articulation angle is very low.

Keywords: transmission efficiency, pendulum, friction losses, measurement, mechanical engineering

(Some figures may appear in colour only in the online journal)

1. Introduction: background to chain testing techniques

Roller chains are a very common and important power transmission device used widely in industry. They are also used widely in transportation systems such as vehicles and elevators. The measurement of transmission efficiency is important to enable the development of higher efficiency chains and for quality control of existing chains. Maintaining and improving the transmission current chain efficiency test rigs typically use an electric motor to turn the drive sprocket and an electric motor to apply a braking torque to the driven sprocket [1] of a chain drive system. Torque or force transducers are used to measure the efficiency of power transmission. These test rigs have several particular disadvantages. Firstly, the accuracy of their efficiency measurement is limited due to friction in the roller bearings and couplings and also due to torque ripples in the motor. In addition, the extra rotating components add inertia which, even with careful characterisation, applies a damping effect and reduces the available measurement bandwidth. Motorised rigs also involve testing of chains with typically over 100 links and hence do not give the option of measuring the efficiency of individual links. Understanding efficiency at link level is important for understanding the effect of variables such as manufacturing tolerances.

Typical chain drives have an efficiency of between 95% and 98%. In order to clearly identify improvements in efficiency it is desirable to measure efficiency to better than 0.1% uncertainty. The prior art in the field of chain drive energy loss measurement tends to focus on mechanised transmission dynamometer methods. Much of the work that has been carried out comes from the domain of commercial and hobbyist cycling, however there have been several academic studies including the much referenced work of Spicer [2] who claims

an accuracy of $\pm 0.2\%$ for his results subject to short term noise and $\pm 0.3\%$ for application to real-world scenarios. In his thesis, Lodge [3] recognises that for these types of rigs, the level of accuracy is dependent on operating regime and presents a series of torque dependent values for accuracy of his experimental apparatus, these range from $\pm 0.3\%$ to $\pm 0.5\%$ over the bulk of the operating envelope of his equipment.

The use of a decaying pendulum to measure energy loss has been successfully applied in a number of fields, either measuring losses in a system via the decay in multiple cycles or during a single swing. For example, Eng *et al* [4] estimated drag coefficients of an underwater vehicle using a model of the vehicle being swung in a tank and measuring decay over multiple cycles. By contrast, Rosenthal and Ungermah [5] incorporated a specimen in the rod of the pendulum itself to examine its dynamic viscoelastic tensile behaviour. This would manifest itself as a change in frequency as well as a decay in amplitude, resulting in quite involved analysis. Medical science often models joints, especially knee joints, as pendula in order to characterise joint stiffness arising from various conditions. For example, Valle *et al* [6] use a pendulum test of the knee to assess rheumatoid arthritis patients, while Noble *et al* [7] use a similar approach in horses. The use of pendulum tests to assess frictional properties through energy loss is used in the British Standard for assessing floor grippiness, BS 7976 [8]. In this last case, the energy loss is measured over a single swing, where a representative rubber sample strikes the floor under test tangentially at bottom dead centre.

2. Methods

2.1. Single link pendulum test (SLPT)

A schematic of the single link pendulum test rig is shown in figure 1. The rig simulates the articulation of a single chain link as it engages and disengages with the sprocket. This articulation is known to be the main source of energy loss in a chain [9].

The pendulum consists of a rigid bar in a vertical orientation with a pivot point at the top and a mass at the bottom. The pivot is a link from a chain under test. When the mass is released from a non-stable initial condition, it oscillates about the pivot, causing the system to continually exchange potential energy with kinetic energy. In practice, the amplitude of the oscillation decays due to energy loss, mainly from sliding friction in the chain link as the pendulum swings.

The initial angular offset of the pendulum must be less than half the circular tooth pitch angle of the sprocket in order to avoid impact with the sprocket teeth. For a 16T sprocket the circular tooth pitch angle is 22.5°, hence an initial angle of less than half this value must be chosen.

If it is assumed that the pendulum consists of a light inextensible rod of length l with a lumped mass m attached at its end, the force balance for the system is written in equation (1). A small amount of rearrangement gives a nonlinear second order ODE, which for small angles where $\sin\theta \approx \theta$ is of the standard form shown in equation (2), allowing the deduction of the undamped natural frequency ω for small angles (3):

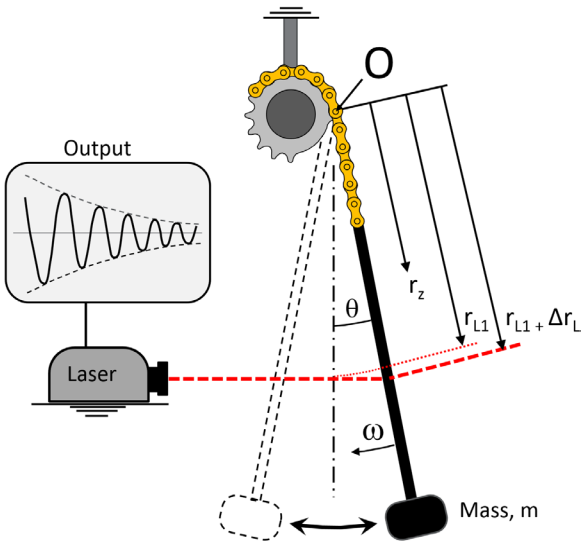

Figure 1. Schematic of the single chain link pendulum test.

$$ml\ddot{\theta} + mg\sin\theta = 0 \tag{1}$$

$$\ddot{\theta} + \omega^2\theta = 0 \tag{2}$$

$$\omega = \sqrt{\frac{g}{l}}. \tag{3}$$

The frictional losses in the chain link can be represented as damping terms in the dynamic equation. In addition, the aerodynamic losses add another nonlinearity, in the form of a quadratic speed term. Although aerodynamic losses are very small, typically less than 1% of the chain losses, they are still modelled and taken into account when calculating transmission efficiency.

The characteristics of the experimental rig are:

- Pendulum length ≈ 0.6 m
- Pendulum frequency ≈ 0.63 Hz
- Initial pendulum angle $< 10°$
- Chain tension: up to 1 kN

The number of oscillations experienced during a decay test depends on the type of chain, the initial offset angle of the pendulum and the mass of the pendulum. Standard roller chains typically experience around 140 oscillations involving sliding friction, whilst a pendulum hung on a knife edge can experience several thousand oscillations.

The motion of the pendulum results in a small force fluctuation in the chain due to the variation of centripetal force with speed. For example, a pendulum with a mass of 50 kg centred at a radius of 0.6 m has a period of approximately 1.55 s and, assuming simple harmonic motion, a peak angular velocity when released from an initial angle of 11° of about 0.7 rad s^{-1}, leading to a force fluctuation with a maximum amplitude of about 5%.

The available chain tension is high enough to simulate most bicycle, motorbike and car timing chain applications. It should be noted that the articulation speeds in the pendulum tests are low compared to those experienced in most power transmission

applications. Typical peak oscillation speeds for the pendula are around 1.0 rad s^{-1}, whilst the driving chain ring of a bicycle at 30 kph articulates the chain at about 3.13 rad s^{-1} and the timing chain in a car may experience articulations in excess of 300 rad s^{-1}. However, power loss is more dependent on chain tension than on speed and lower speeds are more conducive to achieving high accuracy in testing. It is expected that significantly elevated temperatures will affect the chain link coefficient of friction. While the tests in this paper have been conducted at room temperature, if high-temperature performance was of interest, the relatively compact nature of the apparatus, and the absence of externally applied loads or driving forces, means the experiment could be easily replicated in a controlled environment such as a thermal chamber.

2.2. Single link pendulum test dynamic model

The basic premise on which efficiency, η, is calculated is to compare the work done by the bearing losses during a pendulum oscillation with the total system energy at the start of that cycle:

$$\eta = 1 - \frac{WD}{\sum KE + PE|_{\text{start}}} \tag{4}$$

where WD is work done over the cycle and the denominator is the total system energy for the pendulum at the start of the oscillation, which is the sum of the kinetic (KE) and potential (PE) energies at the start of the measuring period. The dynamic equation of motion of the pendulum may be written down as equation (5):

$$J\ddot{\theta} = M_{\text{gravity}}(\theta) - M_{\text{aero}}(\dot{\theta}) - M_{\text{articulation}}(\theta, \dot{\theta}) \tag{5}$$

where $M_{\text{gravity}}(\theta)$ is a driving moment due to pendulum weight and the terms $M_{\text{aero}}(\dot{\theta})$ and $M_{\text{articulation}}(\theta, \dot{\theta})$ are the loss terms due to aerodynamic effects and friction in the chain's pin–bush interface respectively. J is the moment of inertia of the rotating parts of the pendulum rig and $\ddot{\Theta}$ is the angular acceleration of the pendulum system. Without these losses, the pendulum would oscillate indefinitely under the influence of gravity.

The pendulum is set in motion by releasing it from rest at an angle θ from the vertical, providing it with an initial gravitational potential energy (GPE):

$$GPE = mgh = (1 - \cos\theta)mgl. \tag{6}$$

The dynamic equation of the pendulum also implies work done over a cycle. By integrating over one oscillation period, from $t = t0$ to $t = t1$, the work done by the losses in each cycle is given by equation (7), which integrates the power losses P_{aero} and $P_{\text{articulation}}$ with respect to time t from

$$WD = \int_{t0}^{t1} \left[P_{\text{aero}}(\dot{\theta}) + P_{\text{articulation}}(\theta, \dot{\theta})\right] \mathrm{d}t \tag{7}$$

where the instantaneous loss powers during the oscillation are $P_{\text{aero}}(\dot{\theta}) = \dot{\theta}(t)M_{\text{aero}}(\dot{\theta})$ and $P_{\text{articulation}}(\theta, \dot{\theta}) = \dot{\theta}(t)M_{\text{articulation}}(\theta, \dot{\theta})$. By measuring peak speed, at the bottom-dead-centre position of the pendulum, work done may be calculated as the difference in kinetic energy at this point of travel as follows in equation (8):

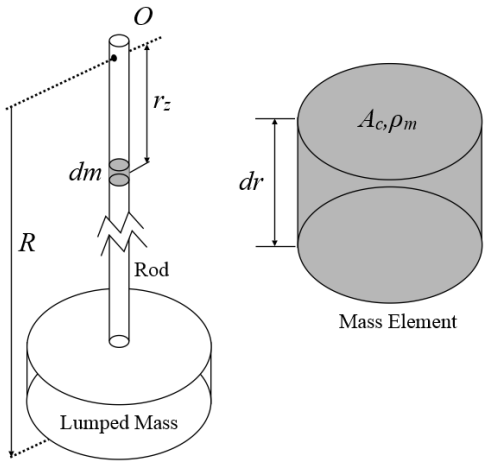

Figure 2. Illustration of a pendulum composed of elemental masses of cross-sectional area A_c, density ρ_m and length $\mathrm{d}r$.

$$WD = \frac{1}{2}J\dot{\theta}^2(t1) - \frac{1}{2}J\dot{\theta}^2(t0). \tag{8}$$

Thus the total work done between the pendulum being released and coming to rest at its stable equilibrium is the sum of the work done overcoming the bearing losses and the small aerodynamic drag, and is equal to the initial potential energy, as follows in equation (9):

$$GPE = \int_{\text{release}}^{\text{rest}} \texttt{Losses}\ \mathrm{d}t. \tag{9}$$

The moment of inertia of the pendulum is calculated by modelling the pendulum as a solid composed of circular cross-sections about a radius of length R with its origin at the centre of rotation O. This arrangement is illustrated in figure 2 and is described as follows in equations (10) and (11):

$$J = \int_0^R r_z^2 \mathrm{d}m \tag{10}$$

$$= \int_0^R \rho_m A_c(r_z) r_z^2 \mathrm{d}r \tag{11}$$

where the standard form of the second moment of inertia in equation (10) is the integral with respect to a unit mass which is then rewritten as a function of the cross-sectional area $A_c(r_z)$ at a given radius r_z and the density of the cross-section ρ_m, so that $\mathrm{d}m = \rho_m A_c(r_z)\mathrm{d}r$. This allows integration with respect to the radius in equation (11).

The instantaneous value of M_{gravity} is given by

$$M_{\text{gravity}} = \int_0^R r_z g \sin\theta \mathrm{d}m \tag{12}$$

$$= \int_0^R \rho_m A_c(r_z) r_z g \sin\theta \mathrm{d}r. \tag{13}$$

The moment about the pivot due to gravity is derived from an expression integrated with respect to mass, along the

pendulum radius in equation (12), where θ is the angle of the pendulum from vertical and g is the gravitational constant. The infinitesimal mass element is written as a function of cross-sectional area and density as in equation (11).

The derivation of the moment due to aerodynamic drag is given in equations (14)–(17), beginning with the integration over the radius of the pendulum of an infinitesimal slice of the tangential aerodynamic drag force acting at a given radius:

$$M_{\text{aero}} = \int_0^R r_z \mathrm{d}F_{\text{aero}}(r_z) \tag{14}$$

$$= \int_0^R r_z \left(\frac{1}{2}\rho_a C_d v_{\tan}^2\right) \mathrm{d}A_f(r_z) \tag{15}$$

$$= \frac{1}{2}\int_0^R r_z \rho_a C_d W_f(r_z) v_{\tan}^2 \mathrm{d}r \tag{16}$$

$$= \frac{1}{2}\int_0^R r_z^3 \rho_a C_d W_f(r_z) \dot{\theta}^2 \mathrm{d}r. \tag{17}$$

The tangential drag force for a slice of pendulum $\mathrm{d}F_{\text{aero}}(r_z) = \left(\frac{1}{2}\rho_a C_d v_{\tan}^2\right)\mathrm{d}A_f(r_z)$ where ρ_a is the density of air, C_d the drag coefficient of the cross-sectional profile of the slice and $v_{\tan} = \dot{\theta} r_z$ is the tangential velocity. The frontal area may be written as $\mathrm{d}A_f(r_z) = W_f(r_z)\mathrm{d}r$ where $W_f(r_z)$ is the width of the cross-sectional profile at radius r_z. These properties allow the expression to be rewritten as equation (17).

The level of the bearing losses is dependent on whether the chain link is in pin-articulation mode or bush-articulation mode. For the sake of simplicity, the expression for frictional loss due to pin-articulation is presented in equation (18). The derivation of this expression and an explanation of the two modes of articulation may be found in sections 2 and 2.4 of this paper where former work by Lodge [9] is reiterated:

$$M_{\text{articulation}} = \frac{F_{\text{pin}}(\theta)\mu_{\text{pin}} r_{\text{pin}}}{\sqrt{1-\mu_{\text{pin}}^2}} \tag{18}$$

where F_{pin} is the load on the link, μ_{pin} is the coefficient of friction of the pin–bush interface and r_{pin} is the radius of the pin. In the case of this test, the load on the link is the combination of weight due to gravity and tension due to centripetal acceleration of the pendulum. For a composite pendulum, the force at the pin due to centripetal acceleration of the pendulum, F_{cen} is calculated by integrating the pendulum elements along the radial axis, presented in equation (19):

$$F_{\text{cen}} = \int_0^R r_z \dot{\theta}^2 \mathrm{d}m. \tag{19}$$

The bearing force in the pin, F_{pin} is equal to the tension in the rod due to the combination of F_{cen} and the component of the weight of the pendulum acting parallel to the shaft:

$$|F_{\text{pin}}(\dot{\theta}, \theta)| = F_{\text{cen}} + mg\cos\theta. \tag{20}$$

The pendulum used in the SLPT system is a composite of cylindrical weights and supports, as illustrated in figure 1. This means that the volume, mass and frontal area of the pendulum may be defined by the radius of its cross-section r_c at a given distance from the pivot r_z. For example, a 0.5 m long circular bar of diameter 0.010 m teminated by a circular weight of thickness 0.010 m and diameter 0.3 m with another, smaller weight of thickness 0.040 m and diameter 0.120 m stacked on it would be written

$$r_c(r_z) = \begin{cases} 0.010, & 0 < r_z \leqslant 0.36 \\ 0.120, & 0.36 < r_z \leqslant 0.40 \\ 0.030, & 0.4 < r_z \leqslant 0.5. \end{cases} \tag{21}$$

The dynamic model presented in this section may be used to compute the expected rate of decay of the pendulum for a given loading, initial condition, coefficient of friction and aerodynamic profile. This allows a comparison with the measured rate of decay, allowing the pin–bush interface losses to be inferred from the measured data.

2.3. Measurement methods

Two different measurement schemes were investigated for observing the states of the pendula during testing. One uses a wireless inertial measurement unit to determine angular (and tangential) accelerations, whilst the other makes use of a Doppler laser vibrometer to measure velocity of the pendula. The main advantage of the inertial unit is that it outputs angular velocity directly. The main advantage of the laser system is that it does not require any equipment to be attached to the pendulum and therefore does not increase the physical size of the pendulum. However, the laser system necessitates some additional data processing. Both systems were tested and found to be of sufficient accuracy but the laser system was chosen in order to keep the pendulum as slim as possible, thus reducing the aerodynamic drag.

The Doppler laser vibrometer used to measure velocity is very accurate. However, it should be noted that the measurement is on a straight line and therefore not always tangential to the pendulum. It may be shown, in equations (22)–(25), that the various parallax errors cancel each other out so that no correction is needed to determine rotational velocity.

The tangential velocity of the part of the pendulum passing through a given horizontal plane is proportional to the distance from the pivot to that plane along the centreline of the pendulum. Therefore,

$$v_{\tan} = \dot{\theta}(r_{L1} + \Delta r_L) \tag{22}$$

where r_{L1} is the radius at which the vertical pendulum crosses the laser line and Δr_L is the change in radius due to the non-vertical attitude of the pendulum, these dimensions are illustrated in figure 1. The radius r_L at which the pendulum and laser line cross may be written as a function of the angle of the pendulum, allowing the

$$v_{\tan} = \dot{\theta}\left(\frac{r_{L1}}{\cos\theta}\right). \tag{23}$$

However, the LDV measures only the horizontal component of the velocity:

$$v_{\text{meas}} = v_{\tan}\cos\theta. \tag{24}$$

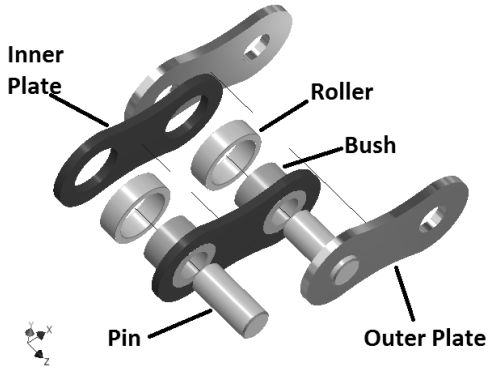

Figure 3. Exploded model of a bush-roller chain inner and outer link showing key components.

The two trigonometric functions cancel one another out as follows:

$$v_{\text{meas}} = \dot{\theta}\left(\frac{r_{L1}}{\cos\theta}\right)\cos\theta = \dot{\theta} r_{L1}. \tag{25}$$

2.4. Chain friction model

The test rigs give a measure of frictional losses without knowledge of the source of friction in the chain drive. However, it is useful to model chain friction because this enables the calculation of the coefficient of friction at the sliding interfaces. This coefficient of friction can be used to predict energy loss and hence efficiency for other drive configurations, speeds and loads.

Most chain drives use a bush-roller chain. These chains consist of two types of link: an outer link of two plates joined by two pins and an inner link made of two plates and two bushes. In addition to the two links there is a roller which acts as a bearing bush between the inner link bush and the sprocket, as illustrated in figure 3.

In a normal power transmission application, one side of the chain is under load whilst the other is slack, or at least is only subjected to pre-load. The chain will wrap on to the driving sprocket on the taught side and off again on the slack side, whilst the opposite is true for the driven sprocket. Work is done due to sliding friction at the interface between pin and bush (or the bush and the roller) when a link articulates under load. At any instant in time there are two links that are articulating under load. One is where the chain articulates off of the driven sprocket and the second is where the chain articulates onto the driving sprocket.

Because there are two types of link in a roller chain, a link articulation can be either a pin articulation or a bush articulation. A schematic of these articulations is shown in figure 4. Sliding takes place between a link that is stationary when viewed from the sprocket's frame of reference and the link which is rotating. When the rotating link is the outer link, the sliding takes place only at the pin–bush interface as shown in figure 4(a). When the rotating link is the inner link, sliding takes place at the bush–roller interface as well as the pin–bush interface, as illustrated in figure 4(b). The reason for this is that the roller is pressed against the sprocket and so the bush must slide against the pin and the roller.

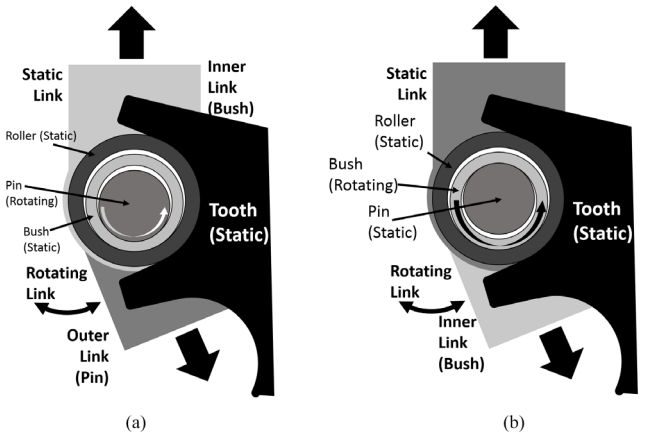

Figure 4. Schematic of pin articulation and bush articulation. (a) Pin articulation. (b) Bush articulation.

The analysis presented in this paper is for the pin articulation case, since this is simpler and provides a clearer illustration of the methods being employed. It should also be noted that it is possible for a chain to experience sliding between the side-plates. However, in a well aligned system, this is negligible so it is ignored for the purposes of this analysis.

The computation of normal load on the interface between either the pin and bush or bush and roller is necessary to allow the calculation of the coefficient of friction from pendulum decay data. Figure 5 shows a vector diagram of the loads at the pin–bush interface. This illustrates the simplest quasi-static model of forces on the link as developed by Binder [10]. The total load transmitted by the link is the vector sum of the tension in the tight span of the chain and in the link wrapped on to the sprocket F_c and F_{cf} and is equal to the vector sum of the normal force at the contact point, F_0 and the tangential friction at the contact point $F_0\mu$, whose combined magnitude is F_{pin}. The relationship between F_{pin} and the normal interface force required in the friction model is given in equations (26) and (27):

$$F_{\text{pin}} = F_c + F_{cf} \tag{26}$$

$$F_0 = \frac{|F_{\text{pin}}|}{\sqrt{1+\mu^2}}. \tag{27}$$

The expression for bearing loss torque in the pin–bush or bush–roller interface is thus derived in equation (28) as the frictional force due to normal load acting at the radius of the pin outer surface, r_{pin}:

$$M_{\text{articulation}} = r_{\text{pin}}\mu F_0 \tag{28}$$

$$M_{\text{articulation}} = \frac{F_{\text{pin}}(\theta)\mu r_{\text{pin}}}{\sqrt{1-\mu^2}}. \tag{29}$$

2.5. Computing Coefficient of friction from the SLPT

For the pin-articulating case, the coefficient of friction at the pin–bush interface may be computed as a function of the

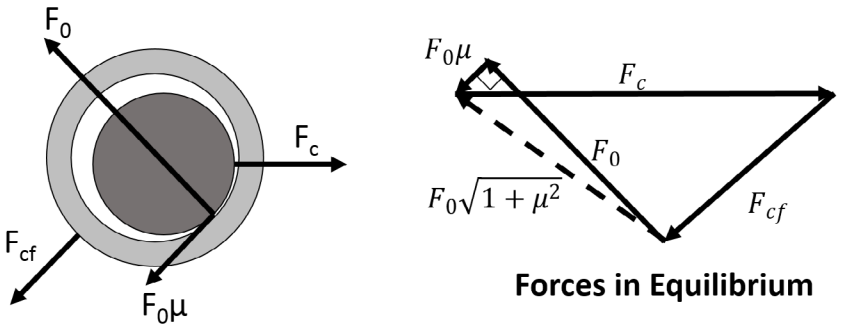

Figure 5. Force summation at pin joint between two links, including the tangential force due to friction.

measured acceleration[1] by simply substituting equation (29) for $M_{\text{articulation}}$ and rearranging equation (5):

$$J\ddot{\theta} + M_{\text{aero}}(\dot{\theta}) - M_{\text{gravity}}(\theta) = M_{\text{articulation}} \tag{30}$$

$$\mu_{\text{pin}} = \frac{F(\dot{\theta},\theta)}{\sqrt{1 + F^2(\dot{\theta},\theta)}} \tag{31}$$

where the forces and moments on the link are grouped in equation (32):

$$F(\dot{\theta},\theta) = \frac{J\ddot{\theta} + M_{\text{aero}} - M_{\text{gravity}}}{r_{\text{bi}}|\mathbf{F}_{\text{pin}}(\theta)|} \tag{32}$$

and $|\mathbf{F}_{\text{pin}}(\theta)|$ is the magnitude of the vector of force on the pin at the current angle θ. The practical implementation of such a design of estimator would ideally be via a Kalman filter or some other similar method to reduce errors due to measurement uncertainty.

The pendulum test gives a direct measurement of the coefficient of friction between the pin and the bush whilst simulating chain articulation at slow speeds. By measuring the decay of the oscillations it is possible to calculate the energy lost at each cycle due to sliding friction and aerodynamic effects. This energy loss can be equated with the work done at the sliding interface of the pin–bush, thus allowing the coefficient of friction to be calculated. The coefficient of friction can then be used to calculate the efficiency of a particular transmission.

The energy lost in each cycle is given by

$$W_{\text{pin}}|_{t_0}^{t_1} = \Delta T - W_{\text{Aero}}|_{t_0}^{t_1} \tag{33}$$

where ΔT is the change in kinetic energy of the system. The peak velocity, shown by the thick bounding line in figures 6 and 7, allows the peak kinetic energy to be computed for each pendulum cycle:

$$\Delta T = \frac{1}{2}J(\dot{\theta}_0^2 - \dot{\theta}_1^2) \tag{34}$$

and W_{Aero} is the work done by aerodynamic drag:

$$W_{\text{Aero}}|_{t_0}^{t_1} = \int_{t_0}^{t_1} \rho_a A_f C_d \dot{\theta}^2 \mathrm{d}t. \tag{35}$$

[1] Note that when using a laser to measure the motion of the pendulum, the measured state is velocity. Thus in order to avoid differentiating a digital output, a system of filters is used to compute the friction coefficient. This arrangement is presented in appendix A.

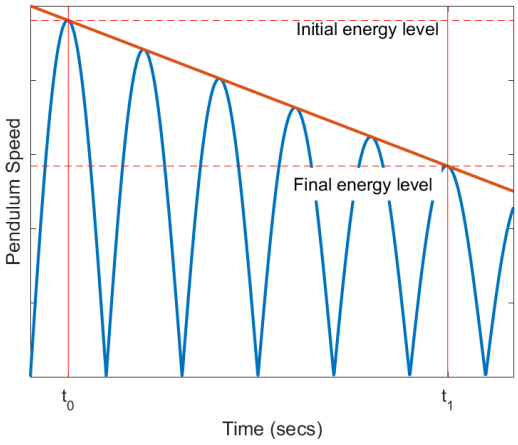

Figure 6. Several oscillations of simple harmonic decay from time t_0 to t_1.

The work done by sliding friction at the pin may also be written as a function of bearing force F_0, bush inner radius r_{bi}, coefficient of friction μ_p and total angular displacement $\alpha_m|_{t_0}^{t_1}$ for a period of time from t_0 to t_1:

$$W_{\text{pin}} = \frac{F_0\mu_p}{\sqrt{1 + \mu_p^2}} r_{\text{bi}}\alpha_m. \tag{36}$$

This may be rearranged to give an expression for coefficient of friction μ_p in terms of measurands from the experiment:

$$\mu_p = \frac{X}{\sqrt{1 - X^2}} \tag{37}$$

where

$$X = \frac{\Delta T - W_{\text{Aero}}|_{t_0}^{t_1}}{r_{\text{bi}}\alpha_m} \tag{38}$$

is the function of angles and angular speeds given in equation (31). The friction values determined in this way correlate well with the experimental work carried out by Spicer [2] and Lodge [3]. Some example results are presented in section 3.3.

3. Results

3.1. Sliding phase of decay

A typical velocity decay profile is shown in figure 7. It may be seen from the figure that there are two different phases of the decay. The first phase of decay, which has a relatively steep

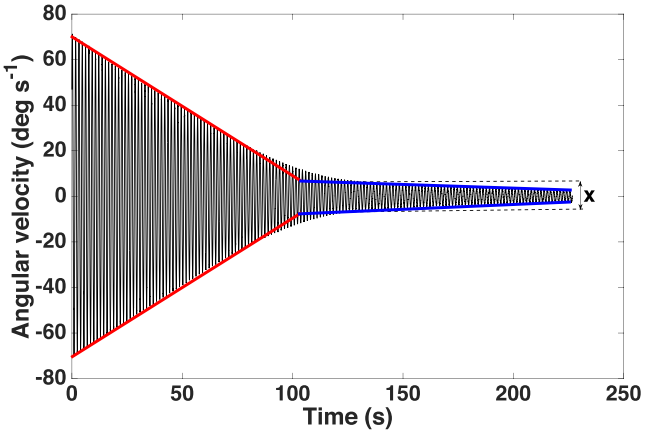

Figure 7. An illustration of a typical decay profile showing the energy consumed by sliding interface friction in the first portion and by rocking only in the second portion.

gradient, is caused by sliding friction at the pin–bush interface whereas the second phase of decay is caused by rolling friction within the link, as it rocks at very low amplitude with no slip.

3.2. Rocking phase of decay

When sliding stops, friction stops the pendulum finding its perfectly vertical position. This residual friction moment then induces a rocking motion which has not previously been reported. The rocking motion continues for many minutes. The initial amplitude of this secondary phase is directly related to the level of sliding friction.

The decay of this secondary phase is a measure of the coefficient of rolling friction. Because the coefficient of rolling friction is an order of magnitude lower than sliding friction, this decay is extremely slow. The amplitude of this second phase of oscillation is typically about 0.5°. The implication of this is that for a chain-sprocket system to be operating in the very low-loss rocking regime only would necessitate a chainring of about 720 teeth. For a $\frac{1}{2}''$ pitch chain, this ring would be about 2.9 m in diameter. For a significantly smaller pitch chain, or a chain with notably reduced pin-size, this dimension would be reduced[2].

3.3. Comparative results and consistency

Table 1 gives an example of single link pendulum test results for five different pin-links of the same chain. The chain was of pitch $0.5''$ and width $0.125''$ and was lubricated according to the manufacturer's guidelines. The results show that there can be significant variation in friction between the different links of a chain. This variation can only be detected with a test rig that deals with single links.

The single link test rig demonstrates very good repeatability of experimental results. When comparing raw results with the mean for a particular test case, the coefficient of determination, R^2 is typically greater than 0.9. An example is given in table 2, listing the coefficients of determination when the results of five identical experiments are compared with the mean of their results. The oscillations are aligned and only a period of decay covered by all five results is compared.

[2] For a knife-edge bearing, the entire motion is in the rocking regime.

Table 1. A comparison of coefficients of friction of five different chain links with a very high level of consistency between link performance, $\sigma = 0.93\%$.

Pin number	Decay time (s)	Rate of angular acceleration ($^\circ s^{-2}$)	Coefficient of friction
1	243.89	−0.2349	0.1090
2	201.28	−0.2212	0.1081
3	200.43	−0.2417	0.1066
4	210.24	−0.2416	0.1070
5	199.94	−0.1919	0.1074

Table 2. Comparison of R^2 values for five repetitions of an SLPT decay experiment.

Test number	R^2 value
1	0.9666
2	0.9569
3	0.9405
4	0.9842
5	0.9571

3.4. Accuracy of measurements

The single link pendulum test is able to have a very high measurement accuracy. With an effective aerodynamic and inertia model, and operating in still air, the accuracy should be limited only by the system used to measure the motion of the pendulum. In a controlled environment, the influence of aerodynamic load on the system is at most 3% of the total loss during the peak speed of the fastest swing. The influence of this term rapidly degrades to be negligible as the peak velocity reduces and it is compensated for by a well characterised aerodynamic model for the rig. This aerodynamic term is computed and accounted for when calculating friction losses.

The most appropriate way to quote the accuracy of the test methods proposed in this paper is to compute an absolute uncertainty based on the accuracy with which the parameters defining the measurand may be determined. In the case of the pendulum, several lengths, masses or densities and aerodynamic characteristics are treated as 'known' parameters to allow the measurand, energy lost in the chain joint, to be computed from the recorded velocity profile of the pendulum.

By using the methods set out in JCGM 100:2008 [11], it is possible to combine the measurement uncertainty of each of the constituent measurements to determine an overall uncertainty. Since it is reasonable to assume that lengths and masses will be measured using the same device, it is necessary to assume that measurements in these two classes will not be fully independent of one another. This necessitates the use of a more general method for combining uncertainties. Thus the formulation used to determine the combined variance should be

Table 3. Typical uncertainty parameters for bearing loss measurement in the SLPT experiments.

Variable (units)	Typical value	Uncertainty
Angular displacement (rad)	0.175	−0.02
Angular velocity (rad s^{-1})	1.1	1.33×10^{-4}
Angular acceleration (rad s^{-2})	1.0	4.79×10^{-3}
Mass (kg)	45	0.001
Length (m)	0.3	0.0005
r_{pin} (mm)	3.4	0.004
Coefficient of friction	0.1	0.000 631

$$u_c^2(y) = \sum_{i=1}^{N} \sum_{j=1}^{N} \frac{\partial f}{\partial x_i} \frac{\partial f}{\partial x_j} u(x_i, x_j) \tag{39}$$

where x_i and x_j are estimates of the measurements X_i and X_j and $u(x_i, x_j)$ is the estimated covariance associated with a pair of measurements x_i and x_j. The expression $Y = f(X_1, X_2, ..., X_N)$ describes the relationship between the measurand and the individual measurable values X_n.

In determining the accuracy of the measurement method for coefficient of friction, both direct Type A and indirect Type B methods have been used. The details of the measurement accuracy calculation are presented in appendix C. Type B methods were used to combine individual measurement accuracies for the different components of the energy loss computation and these are presented in the top part of table 3. Type A methods were then used to determine the overall measurement accuracy of a coefficient of friction calculation, based on the determined input uncertainty model. Details of this process are given in appendix C.

For the case using the parameters in the first part of table 3 to describe measurements of the rig, an uncertainty value of 6.31×10^{-4} is achieved on a measurement of coefficient of friction of 0.1, representing a relative accuracy of about 0.6%. Since the coefficient of friction is related to the efficiency of a chain drive as a factor of the term P_{loss} in equation (40), a small bounds of error on this value translates to a small bounds of error on the overall system efficiency calculation.

Since chain friction losses are typically 2% of transmission power, 0.6% accuracy on friction measurements translates to approximately 0.012% accuracy on the computed transmission efficiency of the drive system.

3.5. Monte-Carlo simulation for method a determination of uncertainty on coefficient of friction calculation

Method A is the more suitable uncertainty computation method for the coefficient of friction because the complete computation of coefficient of friction from its constituent measurements is quite complicated. Since the practical rig may be easily simulated, it is not difficult to use a Monte-Carlo simulation to determine a statistical model for output uncertainty, based on the known uncertainties of the input measurements, thus producing a simulated direct uncertainty calculation by method A.

Table 4.

Measurand	Mean uncertainty	σ uncertainty	Peak uncertainty
F (coefficient of friction)	6.31×10^{-4}	1.73×10^{-4}	9.44×10^{-4}

Simulating the rig requires the implementation of the dynamic models described in section 2.2 of this paper. The measured parameters are modified by adding a randomly generated value according to the uncertainty model for that parameter. The model states and parameters are then used to compute the coefficient of friction as described in equation (31). A normally distributed error based on the performance of the measurement hardware is added to the measured states. A statistical analysis of the outputs after a large number of simulations is provided in table 4. The uncertainty of coefficient of friction determined in this way, with a large enough sample size, may be considered representative of the real performance of the method. The distribution of the noise and errors on the coefficient of friction may be used in online estimation methods for the coefficient of friction parameter, for example, as the statistical model in a Kalman filter or similar estimation algorithm design.

3.6. Aerodynamic influence

An experiment was carried out to confirm that the aerodynamic losses were very small in comparison to sliding friction in the chain. The experiment involved running a test with and without a bluff fairing attached to the pendulum. The fairing increases the total frontal area of the pendulum by 3.2 times, causing an increase in aerodynamic drag. However, it should be noted that the load is spread across a significant radius from the pivot so the increase in load is not proportional to the increase in frontal area.

Five decay tests were carried out on a well lubricated chain with and without a bluff fairing and with almost exactly the same mass. The tests were conducted in the sliding-friction dominated regime. The results showed that there is a slight measurable nonlinearity which can be correlated to a speed squared aerodynamic term. The decay rate data illustrating this are presented in figure 8.

Curves were fitted automatically in Matlab to the two sets of data. Examining figure 8, the constant decay component due to friction and independent of speed is visibly more significant than the velocity squared term from which the aerodynamic contribution may be inferred. The aerodynamic loss, manifesting itself as magnitude of acceleration, without the fairing is slightly less than that with the fairing in place, with v^2 terms of 2.8×10^{-4} and 3.8×10^{-4} respectively.

3.7. Very high efficiency chains

Figure 9 shows decay results for two very high efficiency chains in comparison to a normal roller chain. One of the high efficiency chains consists of a bush with needle roller bearings. The second high efficiency chain consists of a knife-edge bearing in the chain link. The results show that by replacing

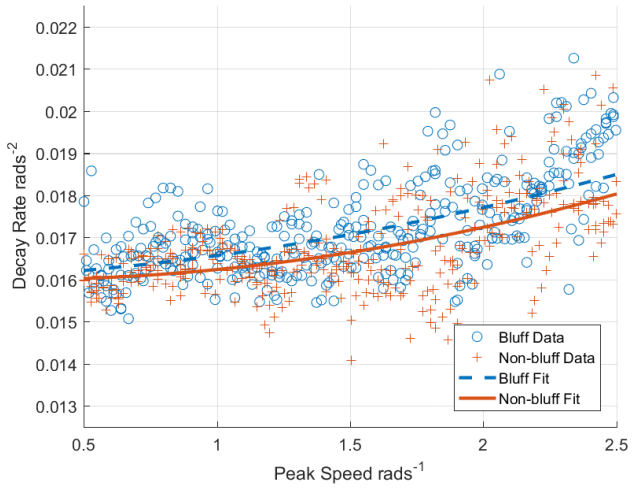

Figure 8. Comparison of decay rates for two pendula with different aerodynamic profiles.

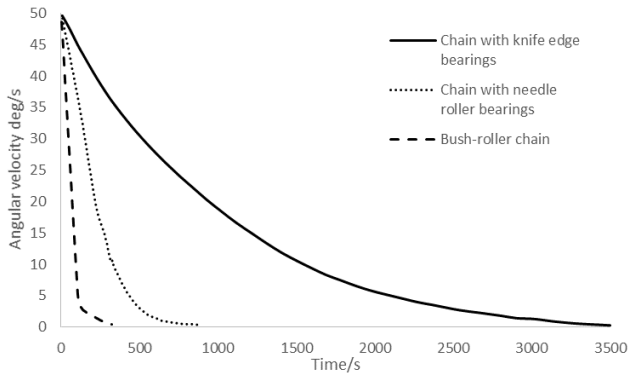

Figure 9. Comparison of decay rates for three pendula with different bearings. The knife edge may be assumed to be decaying mostly due to aerodynamic influence, illustrating clearly how little influence this has on the pendulum compared to a conventional plain bearing.

sliding friction with rolling friction, very low levels of losses are achieved. In the case of the knife-edge bearing, over 3000 pendulum swings were recorded over a period of one hour. This result actually underestimates the performance because aerodynamic drag is a significant factor in the decay of the pendulum for chains with very high efficiency.

4. Discussion

The ability to measure coefficient of friction in a chain link accurately allows models for whole drive-line efficiency to be effectively deployed for assessing power transmission system design. In addition, the development of energy measurement methods using a pendulum system is not restricted to single links or bearings, but may be used to test entire systems.

4.1. Computing chain efficiency

If the coefficient of friction has been calculated then this can be used to predict the efficiency of a drive for any combination of sprockets. The coefficient of friction of the link bearing allows the efficiency of power transmission in the chain to be computed for a given load. A generalised statement of system efficiency is given in equation (40) whilst the expressions for input and loss powers are given in equations (41) and (42) respectively. It is significant to note that since the magnitude of energy dissipation and thus power loss is dependent on the load in the pin, the efficiency of the system is also dependent on the loading case, and also the sizing of the components, since this defines relative angular speeds and loading angles:

$$\eta = 1 - \frac{P_{\text{loss}}}{P_{\text{in}}} \tag{40}$$

$$P_{\text{in}} = F_0 R_1 \dot{\theta}_1 \tag{41}$$

$$P_{\text{loss}} = F_0 \mu \frac{r_{\text{pin}} + r_{\text{bo}}}{2} \frac{\dot{\theta}_1 + \dot{\theta}_2}{2} \tag{42}$$

where R_1 is the radius of the driving sprocket, $\dot{\theta}_1$ and $\dot{\theta}_2$ are the rotational velocities of the driving and driven sprockets respectively, and r_{bo} is the radius of the bush–roller interface; other nomenclature is the same as elsewhere in the paper. An assumption is made that since the pin roller and bush are the same material, the coefficient of friction at the interface is the same and its effect may be averaged as in equation (42). Were this not the case, an adjustment to the formulation would be required. Thus an overall expression for the efficiency of the drive may be written in equation (43):

$$\eta = 1 - \left[\frac{r_{\text{pin}} + r_{\text{bo}}\mu}{2R_1} \left(1 + \frac{N_1}{N_2} \right) \right] \tag{43}$$

where N_1/N_2 is the ratio of the number of teeth on the driving and driven sprockets. The load on the bearing F_0 is also a function of the sprocket size for a given torque. The relationship of the normal load F_0 to the force in individual links is illustrated in figure 5. Numerous models exist of the tension in the links of a chain, including those proposed by Binder [10], Naji and Marshek [12], Troedsson and Vedmar [13, 14] and Lodge [9].

4.2. Testing an entire power transmission system using the pendulum method

The pendulum decay concept can be applied not just to a single link but also to a whole drive system. A schematic of a pendulum decay test rig for a two-sprocket drive system is shown in figure 10. The rig as constructed is shown in figure 11. This test rig has been designed and manufactured and used for testing roller chains. In this case there is a need for bearings to support the two sprocket shafts and these bearings introduce additional friction into the pendulum system. However, ultra-low friction knife-edge bearings are used and their friction level is calibrated. The losses in the knife-edge bearings can be characterised by experimentation by carrying out a pendulum test without chain tension.

This experimental arrangement has the advantage that it decouples tension in the chain from the pendulum dynamics, as the transmission system is tensioned using a turnbuckle in the support frame. The results from this experimental apparatus have an averaging effect on chain losses because there are typically four chain links articulating at any one time.

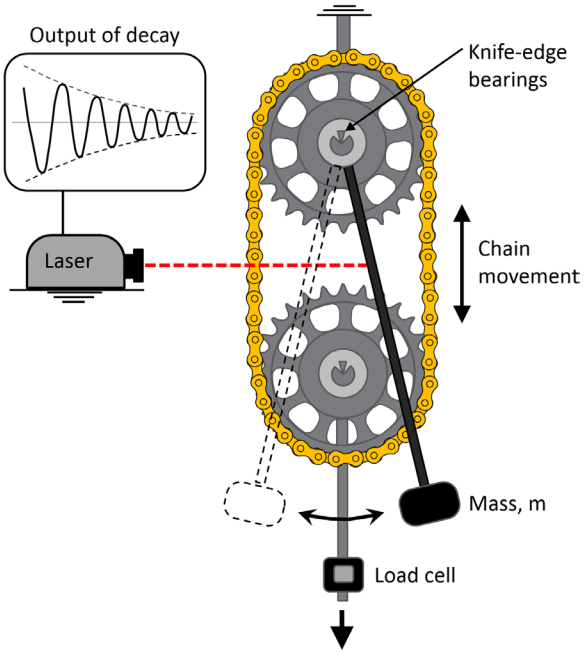

Figure 10. Testing a complete chain drive system using a pendulum.

This method can also be used to test the efficiency belt-drive transmissions since it allows the pre-tension to be altered and does not necessitate the drive being split.

5. Conclusion

A novel pendulum test rig has been developed that gives transmission efficiency measurements without the use of force or torque transducers. Efficiency is calculated from the rate of decay of the swinging pendulum. A friction model for a chain link is presented that allows a coefficient of friction to be derived from the rate of decay of the pendulum. This enables efficiency to be calculated at other loads and speeds for a given chain. The simplicity of the single link pendulum test leads to an accuracy of around 0.6%. This translates to an accuracy of transmission efficiency measurement of typically 0.012%. The new method allows much more accurate measurement of the energy loss in a chain drive than the prior art in this field, whilst much of the work is proprietary and guarded by the industry, Spicer [2] appears to quote ±0.3% for operating under 'normal' conditions.

This level of accuracy of measurement on the numerically small parameter describing coefficient of friction allows the theoretical overall efficiency of a chain drive system to be computed to a high degree of accuracy. The pendulum rig has also allowed the observation of a previously unreported rocking behaviour in the chain links at low articulation angles, rather than the sliding normally experienced at the interface between links. The energy dissipated through rocking is much less than through sliding friction, resulting in a visibly slower deceleration of the pendulum at low oscillation magnitudes. A chain drive designed to maximise efficiency would therefore seek to reduce the articulation angle as much as possible, for example by increasing tooth count on both the driving and driven sprockets.

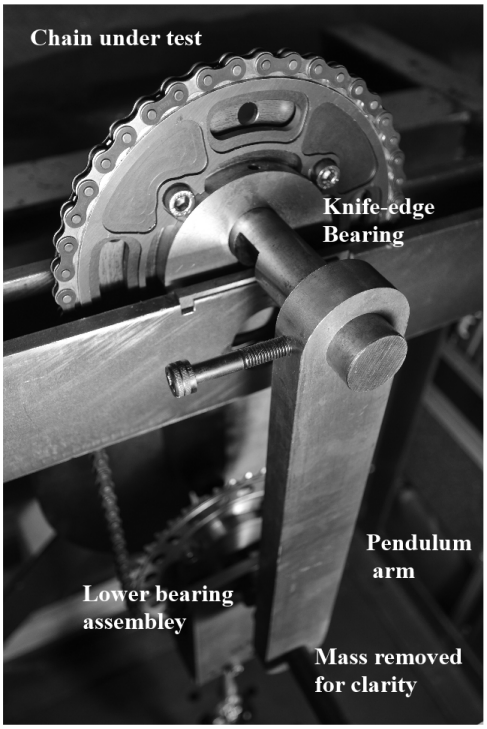

Figure 11. The dual sprocket pendulum test rig for assessing the performance of an entire chain drive.

Acknowledgments

The authors wish to acknowledge the financial, technical and in-kind support of this work by Renold Chain.

Appendix A. Velocity measurement filtering

In order to avoid numerical difficulties arising from differentiating the digital velocity measurement generated by the laser Doppler vibrometer, a system of first order filters may be applied. These are of the form given for a generic value n in equation (A.1), and allow the filtered angular acceleration to be written as a function of the angular velocity and the filtered angular velocity, as in equation (A.2):

$$n_f = k\dot{n}_f - n_f \tag{A.1}$$

$$\ddot{\theta}_f = \frac{\dot{\theta} - \dot{\theta}_f}{k}. \tag{A.2}$$

These expressions may be implemented in a computer simulation using only numerical integration, thus avoiding computational problems with differentiation.

Appendix B. Measurement hardware and associated uncertainties

Table B1 details the manufacturers' quoted accuracy performance for measurement hardware the authors believe to be the

Table B1. Absolute values of uncertainty for representative measurement hardware.

Measurement	Hardware	Abs. uncertainty
Length	Faro Edge CMS	2.40×10^{-5} m
Mass	Adam Eclipse EBL6202i	1.00×10^{-5} kg
Velocity	Polytec OFV-5000 with OFV-505 head, VD-06 velocity decoder	1.00×10^{-8} ms^{-1}
Displacement	Polytec OFV-5000 with OFV-505 head, DD-500 displacement decoder	5.00×10^{-14} m
Pin diameter	Mitutoyo.293-345-30 (293-345) D MATIC EXT. MICROMETER	1.00×10^{-6} m

current state of the art for the measurement ranges required to implement the experiment detailed in this paper.

Appendix C. Method B measurement uncertainty calculation for coefficient of bearing friction

Measurement uncertainty calculations for the SLPT are detailed in this section. Numerical calculations are performed for an example experimental system using measurement equipment the authors believe to represent the current state of the art.

The coefficient of friction is expressed in equation (C.1):

$$Y = \frac{M_{\text{gravity}}(\theta) - M_{\text{aero}}(\dot{\theta}) - J\ddot{\theta}}{r_{\text{pin}}|F_{\text{pin}}(\theta, \dot{\theta})|} \tag{C.1}$$

where all the symbols have the meanings given elsewhere in the paper. For ease of examination of the individual measurements making up each part of this expression, let it be subdivided into parts:

$$Y = \frac{C - B - A}{D} \tag{C.2}$$

where

$$A = J\ddot{\theta} = mr_c^2\alpha \tag{C.3}$$

$$B = M_{\text{aero}}(\dot{\theta}) = A_{CD}r_z^2 w_z \dot{x}^2 \tag{C.4}$$

$$C = M_{\text{gravity}}(\theta) = r_c mg \sin\theta \tag{C.5}$$

$$D = r_{\text{pin}}|F_{\text{pin}}(\theta, \dot{\theta})| = r_{\text{pin}}|mg + F_{\text{cen}}| \tag{C.6a}$$

$$= r_{\text{pin}} m(g^2 + 2gr_c\omega^2 + r_c^2\omega^4)^{\frac{1}{2}} \tag{C.6b}$$

where the pendulum is modelled as a lumped mass m at a radius r_c for simplicity, and the aerodynamic term as a point load defined by the profile $(r_z w_z)$ and aerodynamic coefficients (grouped to $A_{CD} = \rho_a C_d$) acting at a radius r_z. The gravity term is defined in terms of the angle theta, and throughout the expressions (C.3)–(C.6*b*) the higher derivatives of the angle are written as a function of the linear velocity or acceleration measurement (as appropriate) and the radius at which that measurement is taken.

In order to combine the measurement uncertainties for each sub-expression (C.3)–(C.6*b*) according to equation (39) and the guidelines in JCGM 100:2008 [11], the partial derivatives with respect to each measured variable need to be taken. These are presented in equations (C.7*a*)–(C.10*d*):

Table C1. Calculated uncertainty contribution for each part of equation (C.2).

Sub-measurand	% Uncertainty (small magnitude states)
A ($J\alpha$)	0.007 43
B (Aero)	0.028 80
C (Gravity)	0.3541
D (Bearing force)	0.0000 560

$$\frac{\partial A}{\partial m} = r_c^2\alpha \tag{C.7a}$$

$$\frac{\partial A}{\partial r_c} = 2mr_c\alpha \tag{C.7b}$$

$$\frac{\partial A}{\partial \alpha} = mr_c^2. \tag{C.7c}$$

$$\frac{\partial B}{\partial A_{CD}} = r_z^2 w_z \dot{x}^2 \tag{C.8a}$$

$$\frac{\partial B}{\partial r_z} = 2A_{CD}r_z w_z \dot{x}^2 \tag{C.8b}$$

$$\frac{\partial B}{\partial w_z} = A_{CD}r_z^2 \dot{x}^2 \tag{C.8c}$$

$$\frac{\partial B}{\partial \dot{x}} = 2A_{CD}r_z^2 w_z \dot{x}. \tag{C.8d}$$

$$\frac{\partial C}{\partial m} = gr_c(\sin\theta) \tag{C.9a}$$

$$\frac{\partial C}{\partial r_c} = gm(\sin\theta) \tag{C.9b}$$

$$\frac{\partial C}{\partial \theta} = gmr_c\cos\theta. \tag{C.9c}$$

Assuming that the gravitational constant does not introduce any additional uncertainty:

$$\frac{\partial D}{\partial m} = r_{\text{pin}}(g^2 + 2gr_c\omega^2 + r_c^2\omega^4)^{\frac{1}{2}} \tag{C.10a}$$

$$\frac{\partial D}{\partial r_{\text{pin}}} = m(g^2 + 2gr_c\omega^2 + r_c^2\omega^4)^{\frac{1}{2}} \tag{C.10b}$$

$$\frac{\partial D}{\partial r_c} = r_{\text{pin}}\frac{m}{2}(g^2 + 2gr_c\omega^2 + r_c^2\omega^4)^{-1/2}(2g\omega^2 + 2r_c\omega^4) \tag{C.10c}$$

$$\frac{\partial D}{\partial \omega} = r_{\text{pin}}\frac{m}{2}(g^2 + 2gr_c\omega^2 + r_c^2\omega^4)^{-1/2}(4gr_c\omega + 4r_c^2\omega^3). \tag{C.10d}$$

These partial derivatives are combined using a vectorised form of the sum in equation (39), which is summarised in equations (C.11*a*)–(C.11*c*):

$$u_c^2(f) = \frac{\partial \vec{\boldsymbol{F}}}{\partial \boldsymbol{x_n}}[\boldsymbol{U}_N^T\boldsymbol{U}_N \circ \boldsymbol{R}_N]\frac{\partial \vec{\boldsymbol{F}}}{\partial \boldsymbol{x_n}}^T \tag{C.11a}$$

$$\frac{\partial \vec{\boldsymbol{F}}}{\partial \boldsymbol{x_n}} = \begin{bmatrix} \frac{\partial f}{\partial x_1} & \frac{\partial f}{\partial x_2} & \cdots & \frac{\partial f}{\partial x_n} \end{bmatrix} \tag{C.11b}$$

$$\boldsymbol{U}_N = \begin{bmatrix} u_1 & u_2 & \cdots & u_n \end{bmatrix} \tag{C.11c}$$

where f represents the function describing the measurand, x_n is the nth individual measured variable and u_n is the uncertainty associated with that variable. The matrix $\boldsymbol{R}_N$ contains the correlation coefficients $r_n(x_i, x_j)$ for the uncertainties u_i, u_j, where $-1 \leqslant r_n(x_i, x_j) \leqslant +1$ and $r_n(x_i, x_j) = 0$ for uncorrelated measurements:

$$r_n(x_i, x_j) = \frac{u(x_i, x_j)}{u(x_i)u(x_j)}. \tag{C.12}$$

For each of the sub-elements of the measurand expression, the uncertainties and relative uncertainties are as follows in table C1, assuming the state of the art in measurement hardware is employed, as detailed in table B1.

It may be observed from equations (C.7*a*)–(C.10*d*) that the uncertainties of each sub-measurand scale with the states on which they depend. Therefore, to reduce the uncertainty, it is desirable to take measurements at lower amplitudes. Practically this also avoids the risk of chain bounce. It is also important to avoid coefficient of friction measurement in the 'rocking' regime of the chain described in figure 7. With these two requirements accounted for, the uncertainty measurements in this and the following section have been determined for 30 s of oscillation immediately prior to the rocking regime being entered.

ORCID iDs

R Wragge-Morley https://orcid.org/0000-0001-8782-1407
J Yon https://orcid.org/0000-0002-9384-4311

References

[1] Lodge C J and Burgess S C 2000 Experimental measurement of roller chain transmission efficiency *Proc. Int. Conf. Gearing, Transmissions, and Mechanical Systems* pp 603–12
[2] Ehrlich M J, Bernstein J R, Fukuda M, Terada M, Spicer J B and Richardson C K 1999 Effects of frictional loss on bicycle chain drive efficiency *J. Mech. Design* **123** 598–605
[3] Lodge C J 2002 Theoretical and experimental studies of the mechanical behaviour of roller chains *PhD Thesis* University of Bristol
[4] Eng Y, Lau W, Low E, Seet G and Chin C 2008 Identification of the hydrodynamics coefficients of an underwater vehicle using free decay pendulum motion *Eng. Lett.* **16** 326–31
[5] Rosenthal L A and Ungermah A J 1962 A compound pendulum for dynamic viscoelastic property measurements *Polym. Eng. Sci.* **2** 307–12
[6] Valle M S, Casabona A, Sgarlata R, Garozzo R, Vinci M and Cioni M 2006 The pendulum test as a tool to evaluate passive knee stiffness and viscosity of patients with rheumatoid arthritis *BMC Musculoskel. Disorders* **7** 1–12
[7] Noble P, Lumay G, Coninx M, Collin B, Magne A, Lecomte-Beckers J, Denoix J M and Serteyn D 2011 A pendulum test as a tool to evaluate viscous friction parameters in the equine fetlock joint *Veterinary J.* **188** 204–9
[8] Health and Safety Executive 2012 Assessing the slip resistance of flooring a technical information sheet *British Standard* 7976
[9] Lodge C J and Burgess S C 2002 A model of the tension and transmission efficiency of a bush roller chain *Proc. Inst. Mech. Eng. C* **216** 385–94
[10] Binder R C 1956 *Mechanics of the Roller Chain Drive: Based on Mathematical Studies* ed R C Binder (Englewood Cliffs, NJ: Prentice-Hall)
[11] Joint Committee for Guides in Metrology 2008 Evaluation of measurement data—guide to the expression of uncertainty in measurement *Technical Report* JCGM 100
[12] Naji M R and Marshek K M 1983 Analysis of sprocket load distribution *Mech. Mach. Theory* **18** 349–56
[13] Troedsson I and Vedmar L 1999 A method to determine the static load distribution in a chain drive *J. Mech. Des.* **121** 402–8
[14] Troedsson I and Vedmar L 2001 A method to determine the dynamic load distribution in a chain drive *Proc. Inst. Mech. Eng. C* **215** 569–79